On the Chermnykh-Like Problems:

I. The Mass Parameter $\mu = 0.5$

Ing-Guey Jiang[1] and Li-Chin Yeh[2]

[1] Institute of Astronomy, National Central University, Chung-Li, Taiwan

[2] Department of Applied Mathematics, National Hsinchu University of Education, Hsin-Chu, Taiwan

Received _____; accepted _____

ABSTRACT

Following Papadakis (2005)'s numerical exploration of the Chermnykh's problem, we here study a Chermnykh-like problem motivated by the astrophysical applications. We find that both the equilibrium points and solution curves become quite different from the ones of the classical planar restricted three-body problem. In addition to the usual Lagrangian points, there are new equilibrium points in our system. We also calculate the Lyapunov Exponents for some example orbits. We conclude that it seems there are more chaotic orbits for the system when there is a belt to interact with.

Subject headings: planetary systems – stellar dynamics

1. Introduction

Chermnykh's problem concerns the motion of a test particle in the orbital plane of a dumb-bell. This dumb-bell rotates with constant angular velocity n around its mass center. The equations of motion of this test particle are (Chermnykh 1987):

$$\begin{aligned}
\frac{dx}{dt} &= u \\
\frac{dy}{dt} &= v \\
\frac{du}{dt} &= 2nv - \frac{\partial U^*}{\partial x} \\
\frac{dv}{dt} &= -2nu - \frac{\partial U^*}{\partial y},
\end{aligned} \tag{1}$$

where the potential U^* is

$$U^* = -\frac{n^2}{2}(x^2 + y^2) - \frac{\mu_1}{r_1} - \frac{\mu_2}{r_2}, \tag{2}$$

$r_1 = \sqrt{(x+\mu_2)^2 + y^2}$, $r_2 = \sqrt{(x-\mu_1)^2 + y^2}$ and $\mu_1 + \mu_2 = 1$. Usually, the mass parameter $\mu \equiv \mu_2$ and the parameter $n \in [0, \infty)$.

This interesting problem was first analysed in Chermnykh (1987) on the Lyapunov stability of the triangular solutions. Gozdziewski and Maciejewski (1998) studied the Lyapunov stability of the Lagrangian points in the entire range of angular velocity n and mass parameter μ. Recently, Papadakis (2005) investigated the equilibrium points and the zero-velocity curves of this problem. In particular, some families of periodic orbits are studied in great detail. The stability zones are also discussed in that paper.

In general, this important problem has many applications in celestial mechanics (see Gozdziewski and Maciejewski 1999) and chemistry (see Strand and Reinhardt 1979). . When the angular velocity $n = 1$, it is the classical planar restricted three-body problem. When $n = 0$, we get the Euler's problem of two fixed gravitational centers.

On the other hand, because (i) there are many discovered extra-solar planetary systems (Laughlin & Adams 1999, Rivera & Lissauer 2000, Jiang & Ip 2001, Ji et al. 2002), in which about five of them are in binary stars and, (ii) the effect of belts might be important according to some of our previous studies (Yeh & Jiang 2001, Jiang & Yeh 2003, 2004), we here construct a Chermnykh-like problem motivated by these astrophysical applications. In principle, we consider the angular velocity $n > 1$ and its value is determined by the belt's gravitational potential, which is considered as part of the total potential to govern the test particle's motion.

Therefore, we construct our basic model in Section 2. In Section 3, we study the existence of new equilibrium points. We discuss the behavior of the orbits with initial conditions near the new equilibrium points in Section 4 and calculate their values of Lyapunov Exponent in Section 5. Section 6 concludes the paper.

2. The Model

We consider the motion of a test particle influenced by the gravitational force from the central binary and the circumbinary disc.

For convenience, we set the gravitational constant $G = 1$. We assume that two masses of the central binary are μ_1 and μ_2 and choose the unit of mass to make $\mu_1 + \mu_2 = 1$. The separation between two stars in the central binary is set to be unity. The time unit is therefore determined from the above choice.

Under the influence from the belt, when $\mu_1 = \mu_2 = 0.5$, both components of the central binary move on circular orbits at $r = 0.5$ with mean motion, i.e. angular velocity $n = \sqrt{1 - 2f_b(0.5)}$. The gravitational force f_b from the belt is

$$f_b(r) = -\frac{\partial V}{\partial r} = -2\int_{r_i}^{r_o} \frac{\rho(r')r'}{r}\left[\frac{E(\xi)}{r - r'} + \frac{F(\xi)}{r + r'}\right] dr', \tag{3}$$

where

$$\xi = \frac{2\sqrt{rr'}}{r+r'}, \tag{4}$$

$F(\xi)$ and $E(\xi)$ are elliptic integral of the first kind and the second kind and

$$\begin{aligned} F(\xi) &= \int_0^{\pi/2} \frac{1}{\sqrt{1-\xi^2\sin^2\phi'}} d\phi', \\ E(\xi) &= \int_0^{\pi/2} \sqrt{1-\xi^2\sin^2\phi'}\, d\phi'. \end{aligned} \tag{5}$$

(Please see Appendix A for the derivation of Eq.(3).) Hence, the x and y components of gravitational force are

$$\begin{aligned} -\frac{\partial V}{\partial x} &= f_b \frac{x}{r}, \\ -\frac{\partial V}{\partial y} &= f_b \frac{y}{r}, \end{aligned} \tag{6}$$

where f_b is in Eq.(3) and V is the potential from the belt.

Because both components of central binary are doing circular motions, the equation of motion can be written on the frame rotating with the central binary. The equations of motion of this problem are

$$\begin{aligned} \frac{dx}{dt} &= u \\ \frac{dy}{dt} &= v \\ \frac{du}{dt} &= 2nv - \frac{\partial U^*}{\partial x} - \frac{\partial V}{\partial x} \\ \frac{dv}{dt} &= -2nu - \frac{\partial U^*}{\partial y} - \frac{\partial V}{\partial y}, \end{aligned} \tag{7}$$

where the potential U^* is given by Eq.(2). $r_1 = \sqrt{(x+\mu_2)^2+y^2}$ and $r_2 = \sqrt{(x-\mu_1)^2+y^2}$. The Jacobi integral for this system is therefore

$$C_J = -u^2 - v^2 - 2U^* - 2V. \tag{8}$$

The density profile of the belt is

$$\rho(r) = \begin{cases} 0 & \text{when } r < r_i \text{ or } r > r_o, \\ \frac{c}{r^p}\left\{\cos\left[\frac{\pi}{2}\frac{(r-r_a)}{(r_i-r_a)}\right]\right\}^2 & \text{when } r_i < r < r_a, \\ \frac{c}{r^p} & \text{when } r_a < r < r_b, \\ \frac{c}{r^p}\left\{\cos\left[\frac{\pi}{2}\frac{(r-r_b)}{(r_o-r_b)}\right]\right\}^2 & \text{when } r_b < r < r_o, \end{cases} \tag{9}$$

where $r = \sqrt{x^2+y^2}$, c is a constant completely determined by the total mass of the belt and p is a natural number. In this paper, we set $p = 2$, $r_a = r_i + 0.1$, $r_b = r_i + 0.9$, and $r_o = r_i + 1.0$ for all numerical results (Lizano & Shu 1989). It is a power-law profile with smooth edges. Hence, the total mass of the belt is

$$\begin{aligned} M_b &= \int_0^{2\pi}\int_{r_i}^{r_o} \rho(r')r'dr'd\phi \\ &= 2\pi c\left\{\int_{r_i}^{r_a}\frac{1}{r'}\left\{\cos\left[\frac{\pi}{2}\frac{(r-r_a)}{(r_i-r_a)}\right]\right\}^2 dr' + \ln(r_b/r_a)\right. \\ &+ \left.\int_{r_b}^{r_o}\frac{1}{r'}\left\{\cos\left[\frac{\pi}{2}\frac{(r-r_b)}{(r_o-r_b)}\right]\right\}^2 dr'\right\}. \end{aligned} \tag{10}$$

We use r_i and M_b as the controlling parameters of the belt profile. Using Eq.(8), we determine the zero-velocity curves of our system when $r_i = 0.7$ and $M_b = 0.3$, as shown in Figure 1. Because there are elliptic integrals in the potential V, this has to be done numerically and the points are not uniformly distributed on the curves. For the results in Section 4 and Section 5, we always set $r_i = 0.7$ but $M_b = 0.3$ or 0. Following Tancredi et al. (2001), we will integrate the orbits up to 1000 binary period.

3. The Equilibrium Points

We know that there are five equilibrium points (Lagrange points) for the classical restricted three-body problem. Thus, our system shall have five equilibrium points when $M_b = 0$. It would be interesting to investigate the number of equilibrium points when

$M_b > 0$. When there are more than five equilibrium points, we claim that the new equilibrium points exist.

The equilibrium points (x_e, y_e) of System (7) satisfy the following equations:

$$f(x,y) \equiv n^2 x - \frac{\mu_1(x+\mu_2)}{r_1^3} - \frac{\mu_2(x-\mu_1)}{r_2^3} + \frac{x}{r} f_b(r) = 0, \tag{11}$$

$$g(x,y) \equiv n^2 y - \frac{y\mu_1}{r_1^3} - \frac{y\mu_2}{r_2^3} + \frac{y}{r} f_b(r) = 0, \tag{12}$$

Because we consider $\mu_1 = \mu_2 = 0.5$ here, we have:

$$f(x,y) = n^2 x - \frac{(x+0.5)}{2r_1^3} - \frac{(x-0.5)}{2r_2^3} + \frac{x}{r} f_b(r) = 0, \tag{13}$$

$$g(x,y) = n^2 y - \frac{y}{2r_1^3} - \frac{y}{2r_2^3} + \frac{y}{r} f_b(r) = 0, \tag{14}$$

where $r_1 = \sqrt{(x+0.5)^2 + y^2}$ and $r_2 = \sqrt{(x-0.5)^2 + y^2}$.

For convenience, we define

$$h(y) \equiv n^2 - \left[\frac{1}{4} + y^2\right]^{-3/2} + \frac{f_b(r)}{r} \Big|_{(0,y)} \tag{15}$$

and

$$k(x) \equiv n^2 x - \frac{(x+0.5)}{2|x+0.5|^3} - \frac{(x-0.5)}{2|x-0.5|^3} + \frac{x}{r} f_b(r) \Big|_{(x,0)}. \tag{16}$$

We have the following properties for the case of equal-mass binary:

Property 3.1

If (x_e, y_e) is an equilibrium point of System (7), then we have:

either (1) $x_e = 0$ and y_e satisfies $h(y) = 0$

or (2) x_e satisfies $k(x) = 0$ and $y_e = 0$.

Proof: Suppose that (x_e, y_e) is an equilibrium point, thus it satisfies $f(x,y) = 0$ and $g(x,y) = 0$. From Eq.(14), we have

$$y_e \left[n^2 - \frac{1}{2r_1^3} - \frac{1}{2r_2^3} + \frac{f_b(r)}{r} \right] \Big|_{(x_e,y_e)} = 0.$$

Hence, $y_e = 0$ or $[n^2 - \frac{1}{2r_1^3} - \frac{1}{2r_2^3} + \frac{f_b(r)}{r}] \Big|_{(x_e,y_e)} = 0$. We now discuss these two cases separately.

(I) $[n^2 - \frac{1}{2r_1^3} - \frac{1}{2r_2^3} + \frac{f_b(r)}{r}] \Big|_{(x_e,y_e)} = 0$:

Since (x_e, y_e) is an equilibrium point, that is $f(x_e, y_e) = 0$, we have:

$$\begin{aligned} 0 &= f(x_e, y_e) = x_e \left[n^2 - \frac{1}{2r_1^3} - \frac{1}{2r_2^3} + \frac{f_b(r)}{r} \right] - \frac{1}{4r_1^3} + \frac{1}{4r_2^3} \\ &= \frac{1}{4} \left[-\frac{1}{r_1^3} + \frac{1}{r_2^3}, \right]. \end{aligned} \tag{17}$$

Thus, $r_1 = r_2$, i.e. $(x_e + 0.5)^2 + y_e^2 = (x_e - 0.5)^2 + y_e^2$. Hence $x_e = 0$. We have $r_1 = r_2 = \sqrt{1/4 + y_e^2}$ and thus, $h(y_e) = n^2 - [\frac{1}{4} + y_e^2]^{-3/2} + \frac{f_b(r)}{r} \Big|_{(0,y_e)} = [n^2 - \frac{1}{2r_1^3} - \frac{1}{2r_2^3} + \frac{f_b(r)}{r}] \Big|_{(0,y_e)} = 0$. Therefore, $x_e = 0$ and y_e satisfies $h(y) = 0$ for the equilibrium point (x_e, y_e).

(II) $y_e = 0$:

$f(x_e, y_e) = f(x_e, 0) = k(x_e) = 0$ for the equilibrium point (x_e, y_e). Thus, x_e satisfies $k(x) = 0$ and $y_e = 0$. $\diamondsuit$

Property 3.2

(A) If y_e satisfies $h(y) = 0$, then $(0, y_e)$ is an equilibrium point of System (7).

(B) If x_e satisfies $k(x) = 0$, then $(x_e, 0)$ is an equilibrium point of System (7).

Proof of (A): Suppose that y_e is one of the roots of $h(y)$, i.e. $h(y_e) = 0$ and we set $x_e = 0$. Because $g(0, y_e) = y_e h(y_e) = 0$. By Eq.(13), $f(0, y_e) = -\frac{1}{4}[\frac{1}{4} + y_e^2]^{-3/2} + \frac{1}{4}[\frac{1}{4} + y_e^2]^{-3/2} = 0$. Thus, $(0, y_e)$ is the equilibrium point of System (7). $\diamondsuit$

Proof of (B): Suppose that x_e is one of the roots of $k(x)$, i.e. $k(x_e) = 0$ and we set $y_e = 0$. Since $y_e = 0$, it is trivial that $g(x_e, 0) = 0$. Because $k(x_e) = 0$, $f(x_e, 0) = k(x_e) = 0$. Thus, $(x_e, 0)$ is the equilibrium point of System (7). $\diamondsuit$

Because of the above two properties, in stead of searching the roots for two-variable functions $f(x, y)$ and $g(x, y)$ to determine the equilibrium points on the $x - y$ plane, we only need to find the roots of one variable functions $h(y)$ and $k(x)$ to get all the equilibrium

points of System (7) when the mass parameter $\mu = 0.5$. Therefore, we numerically solve both $h(y) = 0$ and $k(x) = 0$ and find out the number of equilibrium points for different given parameters. The numerical scheme of root finding is the Van Wijngaarden-Dekker-Brent Method (Brent 1973). This is an excellent algorithm recommended by Press et al. (1992). We set a high level of accuracy that the maximum error is 10^{-8} for the locations of equilibrium points on both x-axis and y-axis.

Figure 2 shows the results on the $r_i - M_b$ plane. That is, we numerically search the solution of $k(x) = 0$ and $h(y) = 0$ for different (r_i, M_b), where $0.5 < r_i \leq 1$ and $0.001 \leq M_b \leq 0.35$. The grid size is 0.01 for r_i and is 0.02 for M_b. Those (r_i, M_b) with new equilibrium points are marked by full triangle points.

We find that the region with new equilibrium points is itself a triangle. To have new equilibrium points, the mass of the belt has to be larger than 0.15 and r_i is somewhere between 0.7 and 0.8.

It is not surprising that there are more equilibrium points in our system because the potential field of whole system is more complicated than the classical restricted three-body problems and thus there are more possibilities that gravitational forces from different components can balance each other.

4. The Orbits

Since we have discovered new equilibrium points for particular regions of $r_i - M_b$ plane for our system, it would be interesting to investigate the orbital behavior around these new equilibrium points.

From Figure 2, we notice that when $M_b = 0.3$, $r_i = 0.7$, we could have new equilibrium points. We thus use this as a standard case. At the y-axis, we explicitly determine the

locations of all equilibrium points, which are at $(x_e, y_e) = (0, \pm 0.73), (0, \pm 0.77), (0, \pm 1.05)$, in addition to the usual $L1$ point at $(0, 0)$. (We find that all new equilibrium points are at y-axis because of the choice $\mu_1 = \mu_2 = 0.5$.)

To understand the properties of these equilibrium points at the y-axis, we numerically calculate the orbits with initial conditions very close to these points. There are four initial conditions in this paper, i.e.

(a) Initial Condition L1: $(x, y, u, v) = (\epsilon, 0, 0, 0)$,

(b) Initial Condition E1: $(x, y, u, v) = (\epsilon, 0.73, 0, 0)$,

(c) Initial Condition E2: $(x, y, u, v) = (\epsilon, 0.77, 0, 0)$,

(d) Initial Condition E3: $(x, y, u, v) = (\epsilon, 1.05, 0, 0)$,

where $\epsilon = 0.001$.

Figure 3 is the orbits on the $x - y$ plane for these four initial conditions with $M_b = 0.3$. There are four panels, i.e. panel (a) is for Initial Condition L1, panel (b) is for Initial Condition E1, panel (c) is for Initial Condition E2 and panel (d) is for Initial Condition E3. To have the idea about the disc's influence, we also integrate the orbits with these four initial conditions while the disc mass $M_b = 0$ as shown in Figure 4.

For Initial Condition L1, Figure 3(a) shows that the orbit fills the Roche lobe, i.e. the zero-velocity curve passing the L1 point. The test particle is gravitational bound to one of the star because it probably has less initial total energy than those ones in Figure 3(b)-(d). Figure 4(a) shows that the result is similar when $M_b = 0$.

For Initial Condition E1, Figure 3(b) shows that the test particle moves randomly at the beginning and then steadily move out of the region of central binary. Figure 4(b) shows that the test particle drifts away from the initial location regularly.

For Initial Condition E2, Figure 3(c) is similar to Figure 3(b) but the test particles

move more chaotically in the central region and then move out slowly at the first stage and more quickly finally. Figure 4(c) is very similar to Figure 4(b).

For Initial Condition E3, Figure 3(d) shows that the test particle is always close to the equilibrium point and moving on a regular periodical orbit. The equilibrium point could be a neutral stable point. Figure 4(d) shows that the test particle is on a complicated orbit and drifts away from the central region slowly.

We notice that the orbits in Figure 3(a) and Figure 4(a) are surrounding one star only. Most other orbits show that the test particles move spirally outward from the central region except the one in Figure 3(d).

5. Lyapunov Exponent

In addition to analyze the orbits themselves, we calculate these orbits' Lyapunov Exponents to understand how sensitively dependent on the initial conditions. In general, the larger value of Lyapunov Exponent means more sensitively dependent on the initial conditions.

Our procedure to calculate the Lyapunov Exponent was from Wolf et al. (1985). The maximum Lyapunov Exponent is defined by $\gamma = \lim_{t\to\infty}\chi(t)$, where $\chi(t)$ is the Lyapunov Exponent Indicator. The system is chaotic if $\gamma > 0$ or otherwise regular. However, it is not possible to take $t \to \infty$ in practice. We numerically determine the Lyapunov Exponent Indicator $\chi(t)$ and usually plot $\ln\chi(t)$ as function of $\ln t$ after the evolution is followed up to some time. If the curve (or the envelope of the curve) on the $\ln t - \ln\chi(t)$ plane shows a negative constant slope, the system is regular, otherwise it is chaotic.

Figure 5(a)-(d) are the results of Lyapunov Exponent for Initial Condition L1, E1, E2 and E3 respectively. There are two curves in each panel, where solid curve is the result of

$M_b = 0.3$ and dotted curve is the result of $M_b = 0$.

From these results, we notice that the dotted curves in Figure 5(b)-(c) and the solid curve in Figure 5(d) show negative constant slopes. Thus, when $M_b = 0$, the orbits of Initial Condition E1 and E2 are likely to be regular. When $M_b = 0.3$, only the orbit of Initial Condition E3 is likely to be regular. This is probably due to that the equilibrium point close to Initial Condition E3 is neutral stable. Note that the solid curves in Figure 5(b)-(c) are shorter because the test particles were ejected and the calculations were stopped when the distances were larger than 10^4 from the central region.

We can also notice that, in Figure 5(a), the solid curve is always higher than the dotted curve. That is, the values of Lyapunov Exponent Indicator of the orbit with Initial Condition L1 when $M_b = 0.3$ are always larger than the one of the orbit with Initial Condition L1 when $M_b = 0$. To summarize, the existence of belt seems to make the system to have more chaotic orbits.

6. Concluding Remarks

We have provided the equations for a model which includes the gravitational influence from a belt around the central binary. We find that, in addition to the usual Lagrange points, there are new equilibrium points on the y-axis when each mass of the components of the binary is equal to 0.5. To study the orbits around these new equilibrium points, we calculate the orbits and their Lyapunov Exponents with four different initial conditions. It seems that the system could have more chaotic orbits when there is a belt.

Acknowledgements

We are grateful to the National Center for High-performance Computing for computer time and facilities. This work is supported in part by the National Science Council, Taiwan, under Ing-Guey Jiang's Grants NSC 94-2112-M-008-010 and also Li-Chin Yeh's Grants NSC 94-2115-M-134-002.

REFERENCES

Brent, R. P., 1973, Algorithms for Minimization without Derivatives, Englewood Cliffs, NJ: Prentice-Hall.

Byrd, P. F., Friedman, M. D., 1971, Handbook of Elliptic Integrals for Engineers and Scientists, 2nd Edition, Springer-Verlag.

Chermnykh, S. V., 1987, Vest. Leningrad Univ. 2, 10.

Gozdziewski, K., Maciejewski, A. J., 1998, Celestial Mech. Dynam. Astronom., 70, 41.

Gozdziewski, K., Maciejewski, A. J., 1999, Celestial Mech. Dynam. Astronom., 75, 251.

Ji, J., Li, G., Liu, L., 2002, ApJ, 572, 1041.

Jiang, I.-G., Ip, W.-H., 2001, A&A, 367, 943.

Jiang, I.-G., Yeh, L.-C., 2003, Int. J. Bifurcation and Chaos, 13, 617.

Jiang, I.-G., Yeh, L.-C., 2004, Int. J. Bifurcation and Chaos, 14, 3153.

Laughlin, G., Adams, F. C., 1999, ApJ, 526, 881.

Lizano, S., Shu, F. H., 1989, ApJ, 342, 834.

Papadakis, K. E., 2005, Astrophysics and Space Science, 299, 67.

Press, W. H. et al., 1992, Numerical recipes in Fortran Cambridge: Cambridge University Press.

Rivera, E. J., Lissauer, J. J., 2000, ApJ, 530, 454.

Strand, M. P., Reinhardt, W. P., 1979, J. Chem. Phys., 45, 441.

Tancredi, G., Sànchez, A., Roig, F., 2001, AJ, 121, 1171.

Wolf, A., Swift, J. B., Swinney, H. L., Vastano, J. A., 1985, Physica 16D, 285.

Yeh, L.-C., Jiang, I.-G., 2001, ApJ, 561, 364.

This manuscript was prepared with the AAS LaTeX macros v4.0.

A. Gravitational Force from the Belt f_b

Let $F(\xi)$ be the elliptic integral of the first kind and assume

$$\xi = \frac{2\sqrt{rr'}}{r+r'}. \tag{A1}$$

By $\sin^2 A = \frac{1}{2}(1-\cos 2A)$, we have

$$\begin{aligned} F(\xi) &= \int_0^{\pi/2} \frac{1}{\sqrt{1-\xi^2\sin^2\phi'}} d\phi' \\ &= (r+r')\int_0^{\pi/2} \frac{1}{\sqrt{r^2+r'^2+2rr'\cos(2\phi')}} d\phi' \\ &= \frac{(r+r')}{2}\int_0^{\pi} \frac{1}{\sqrt{r^2+r'^2+2rr'\cos(\theta)}} d\theta \\ &= \frac{(r+r')}{2}\int_0^{\pi} \frac{1}{\sqrt{r^2+r'^2-2rr'\cos(\phi)}} d\phi. \end{aligned} \tag{A2}$$

Therefore, from Equation (A2), we have

$$\begin{aligned} &\int_0^{2\pi} \frac{1}{\sqrt{r^2+r'^2-2rr'\cos(\phi)}} d\phi \\ &= 2\int_0^{\pi} \frac{1}{\sqrt{r^2+r'^2-2rr'\cos(\phi)}} d\phi \\ &= \frac{4F(\xi)}{r+r'}. \end{aligned} \tag{A3}$$

The gravitational potential is

$$\begin{aligned} V(r) &= -\int_{r'}\int_0^{2\pi} \frac{\rho'(r')r'}{\sqrt{r^2+r'^2-2rr'\cos(\phi')}} dr'd\phi' \\ &= -4\int_{r'} \frac{F(\xi)\rho'(r')r'}{r+r'} dr', \end{aligned} \tag{A4}$$

where Equation (A3) has been used. Now we differentiate this potential with respect to r to get the gravitational force, so

$$f_b = -\frac{\partial V}{\partial r}$$

$$
\begin{aligned}
&= 4\int_{r'} \frac{\frac{dF(\xi)}{d\xi}\frac{\partial\xi}{\partial r}\rho'(r')r'}{r+r'}dr' \\
&+ 4\int_{r'} F(\xi)\rho'(r')r'\frac{\partial}{\partial r}\left(\frac{1}{r+r'}\right)dr'. \qquad \text{(A5)}
\end{aligned}
$$

Let $E(\xi)$ be the elliptic integral of the second kind and $\xi' = \sqrt{1-\xi^2}$. Since $F(\xi)$ is the elliptic integral of the first kind, from Byrd & Friedman (1971), we have

$$
\frac{dF(\xi)}{d\xi} = \frac{E - \xi'^2 F(\xi)}{\xi\xi'^2} = \frac{E}{\xi(1-\xi^2)} - \frac{F}{\xi}. \qquad \text{(A6)}
$$

By Equation (4) and (A6), we calculate

$$
\begin{aligned}
\frac{dF(\xi)}{d\xi}\frac{\partial\xi}{\partial r} &= \left[\frac{E}{\xi(1-\xi^2)} - \frac{F}{\xi}\right]\sqrt{\frac{r'}{r}}\frac{r'-r}{(r+r')^2} \\
&= -\frac{E(r+r')}{2r(r-r')} + \frac{F(r-r')}{2r(r+r')}. \qquad \text{(A7)}
\end{aligned}
$$

We substitute Equation (A7) into Equation (A5), so we have

$$
\begin{aligned}
f_b &= -\frac{\partial V}{\partial r} \\
&= -2\int_{r'} \frac{\rho(r')r'}{r}\left[\frac{1}{r-r'}E(\xi) + \frac{1}{r+r'}F(\xi)\right]dr'. \qquad \text{(A8)}
\end{aligned}
$$

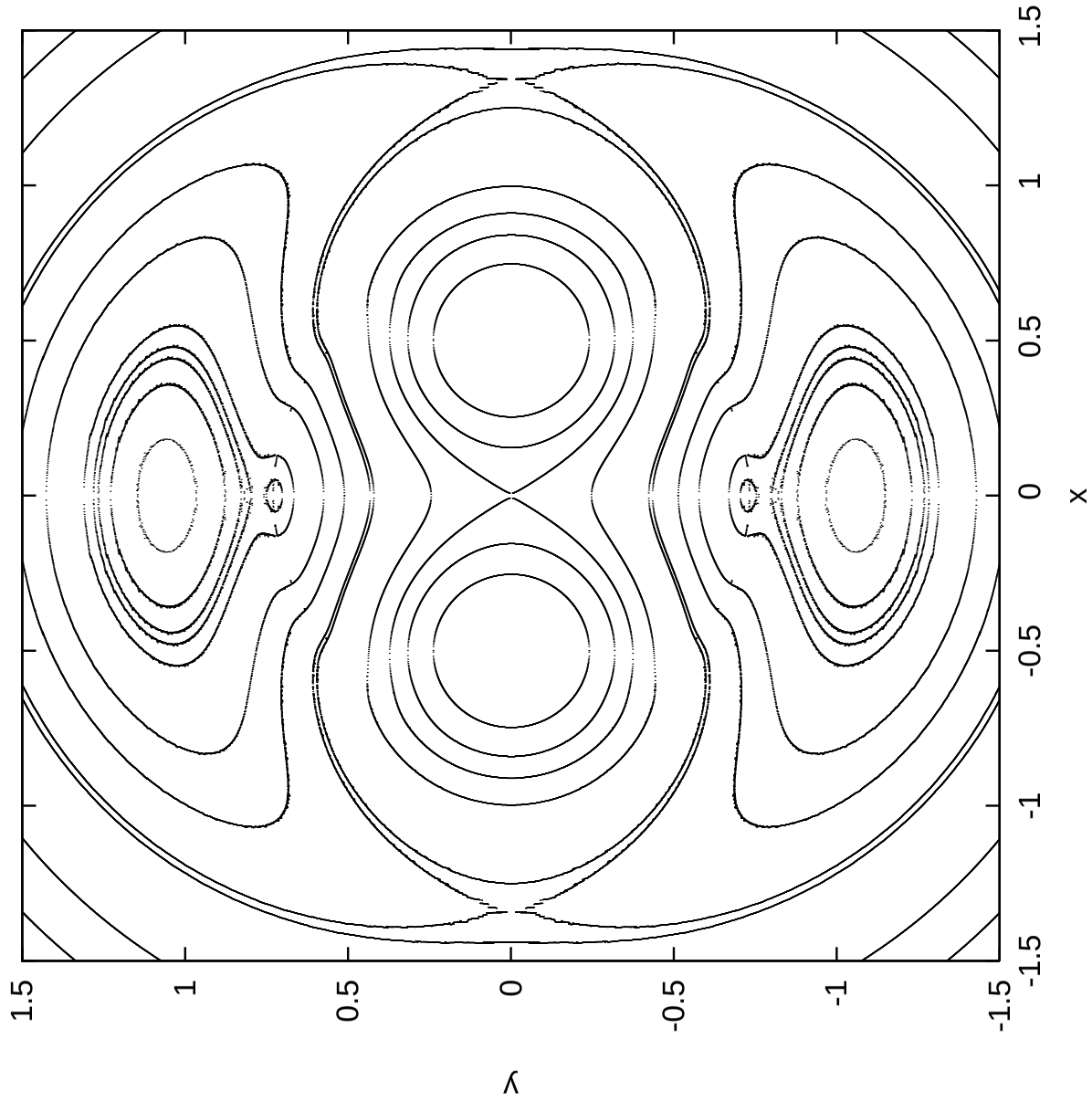

Fig. 1.— The zero-velocity curves of the system when $r_i = 0.7$ and $M_b = 0.3$.

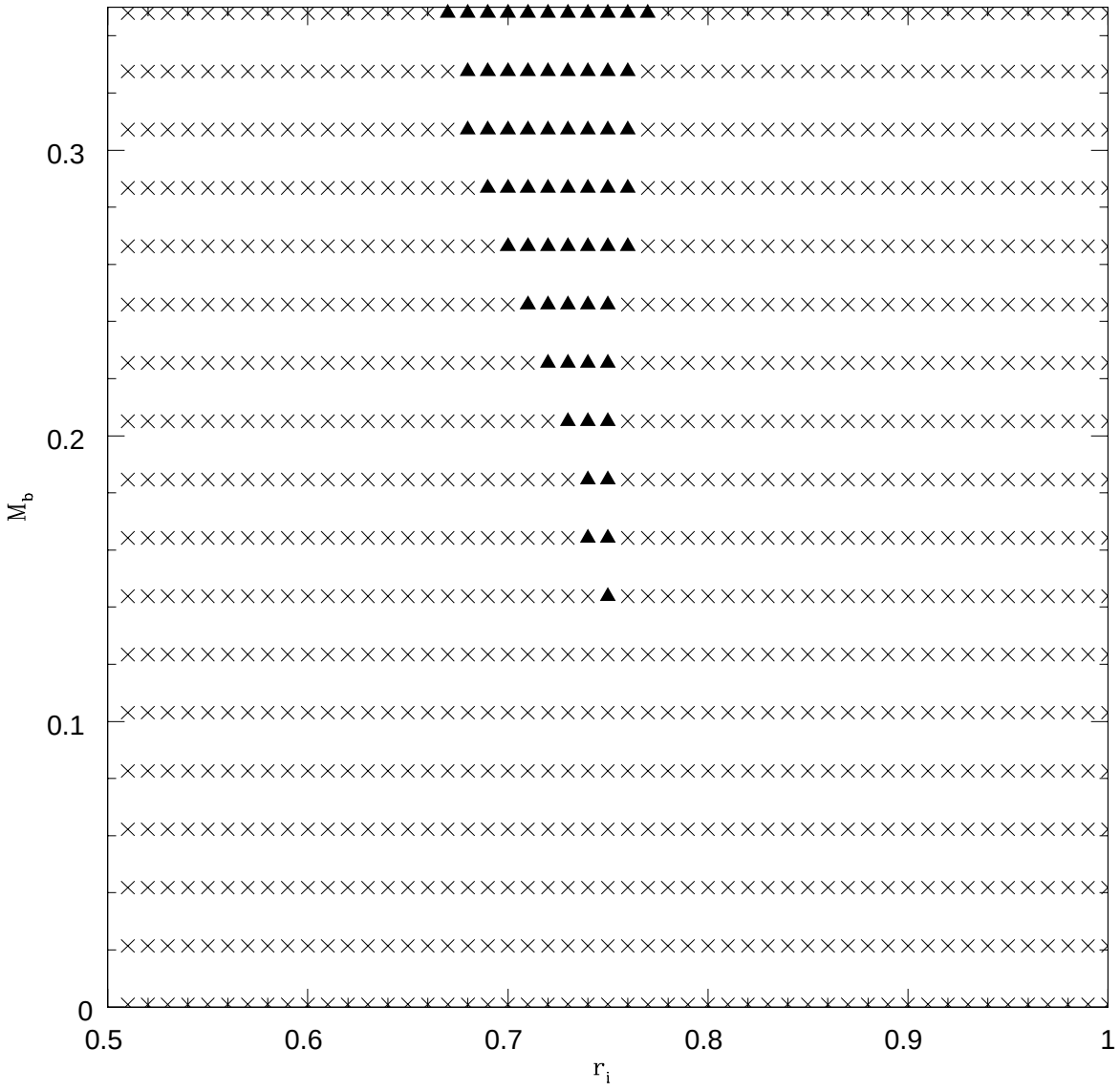

Fig. 2.— The results of the numerical survey on equilibrium points. Those (r_i, M_b) with new equilibrium points are marked by full triangle points.

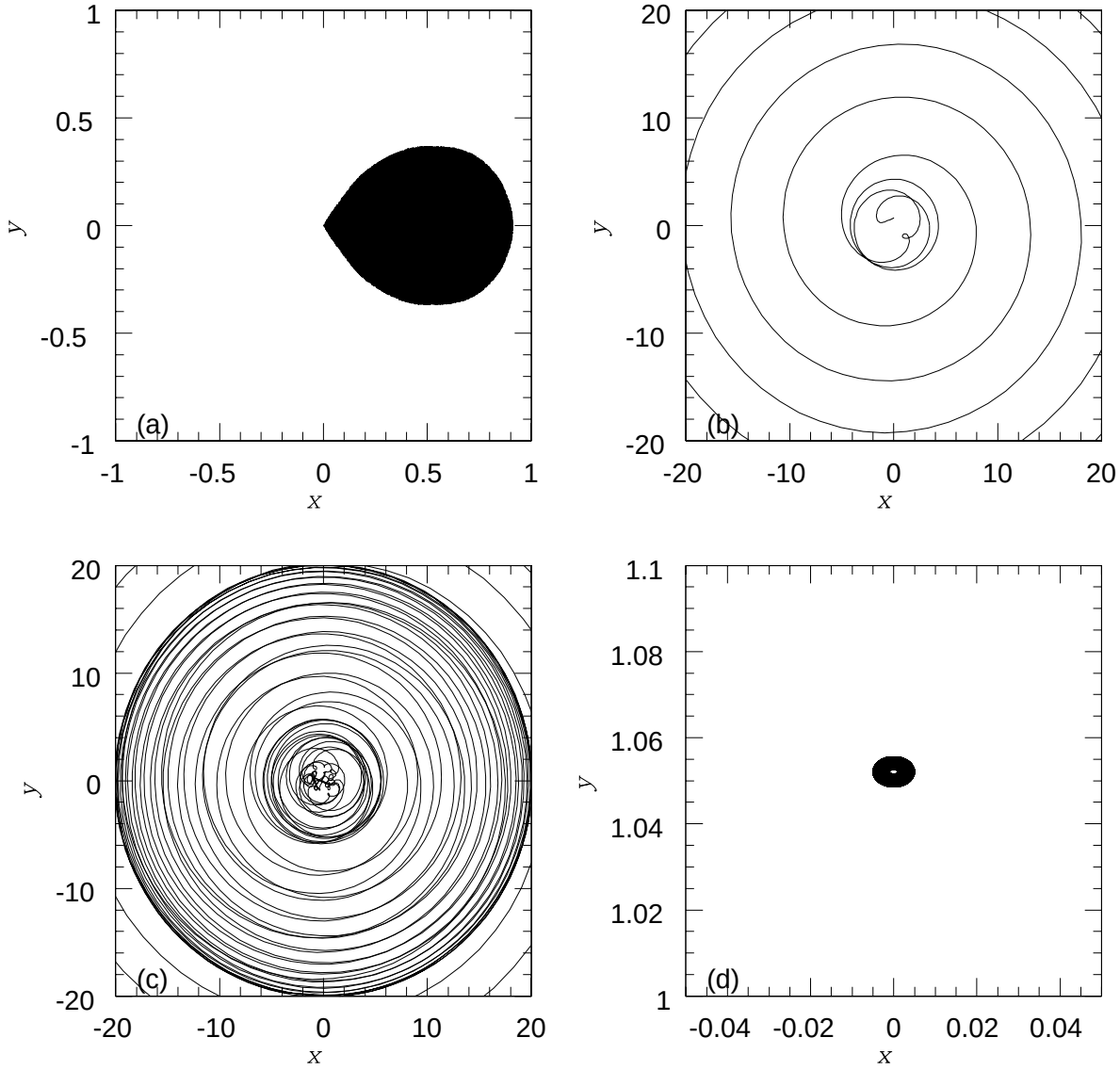

Fig. 3.— The orbits when the disc mass $M_b = 0.3$. Each panel is for different initial conditions, i.e. (a) Initial Condition L1; (b) Initial Condition E1; (c) Initial Condition E2; (d) Initial Condition E3.

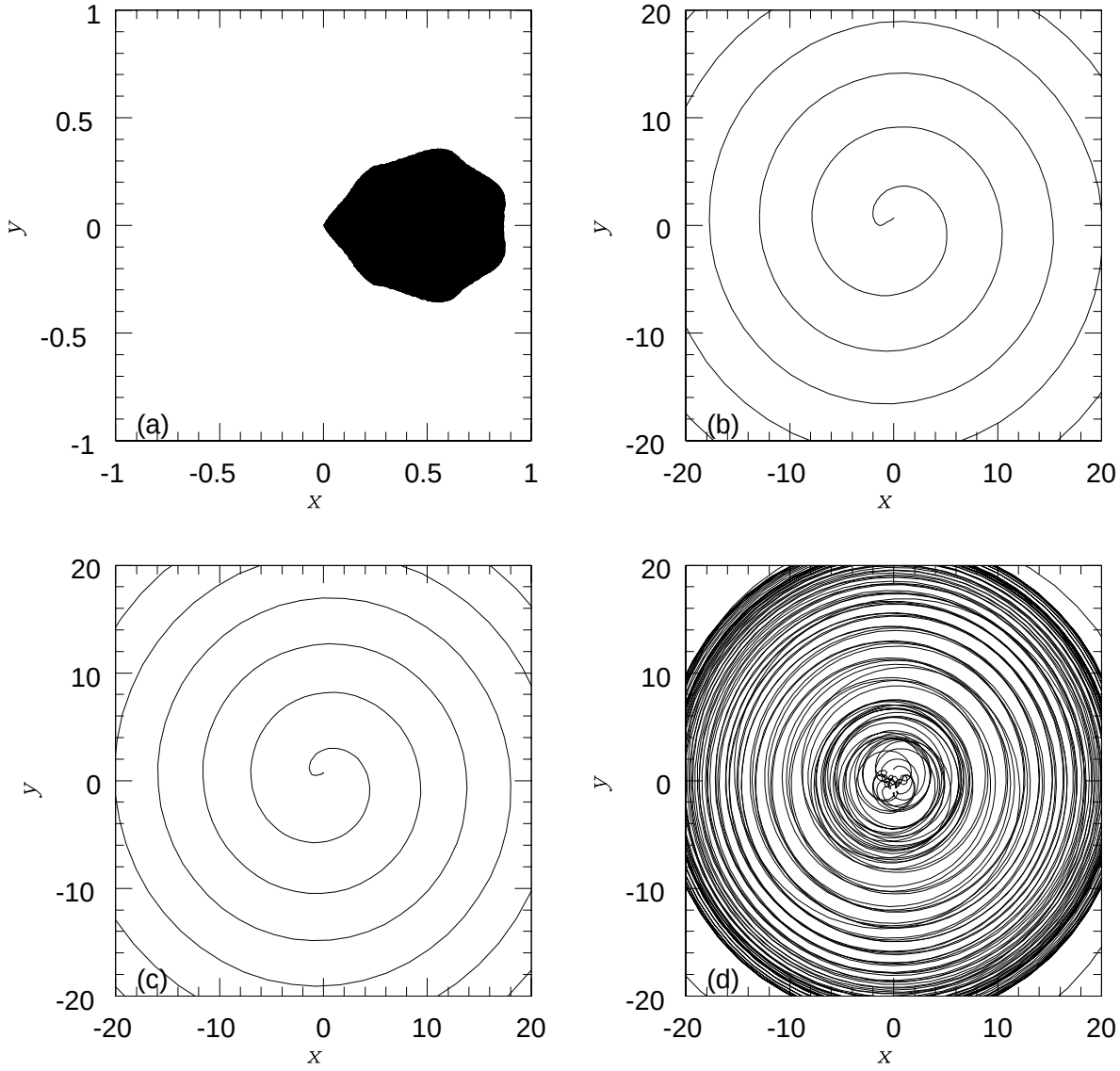

Fig. 4.— The orbits when the disc mass $M_b = 0$. Each panel is for different initial conditions, i.e. (a) Initial Condition L1; (b) Initial Condition E1; (c) Initial Condition E2; (d) Initial Condition E3.

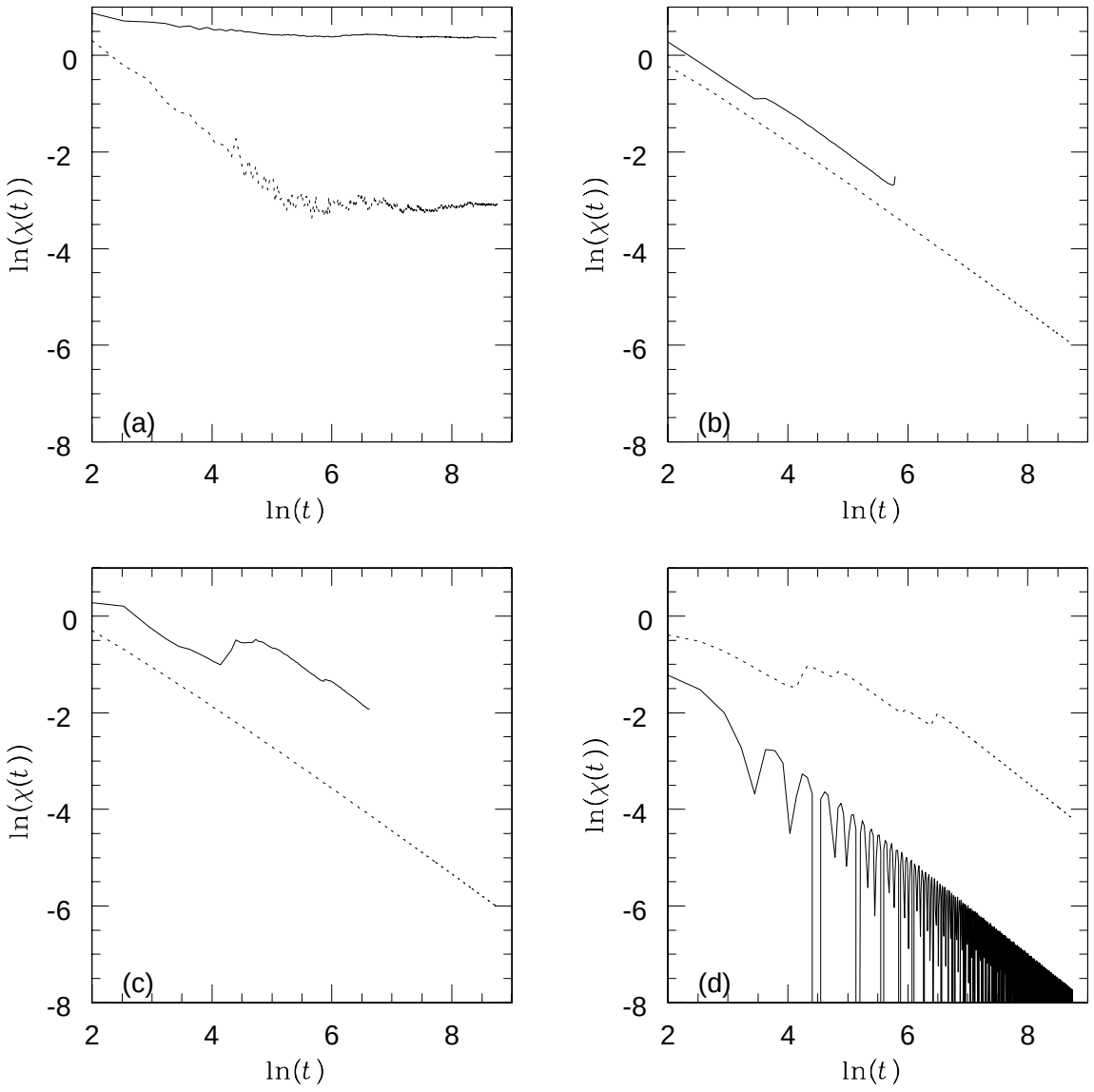

Fig. 5.— Lyapunov Exponent for different disc mass and initial condition, i.e. Panel (a) is for Initial Condition L1; Panel (b) is for Initial Condition E1; Panel (c) is for Initial Condition E2; Panel (d) is for Initial Condition E3. In each panel, solid curve is for $M_b = 0.3$, dotted curve is for $M_b = 0$.